Title

A Radical Intermediate in Bacillus subtilis QueE during Turnover with the Substrate Analogue 6-Carboxypterin

Journal

Journal of the American Chemical Society, 140(5)

ISSN

0002-7863

Authors

Wilcoxen, Jarett
Bruender, Nathan A
Bandarian, Vahe
et al.

Publication Date

2018-02-07

DOI

10.1021/jacs.7b10860

Peer reviewed

HHS Public Access

Author manuscript

J Am Chem Soc. Author manuscript; available in PMC 2019 March 05.

Published in final edited form as:

J Am Chem Soc. 2018 February 07; 140(5): 1753–1759. doi:10.1021/jacs.7b10860.

A Radical Intermediate in *Bacillus subtilis* QueE During Turnover With the Substrate Analog 6-Carboxypterin

Jarett Wilcoxen[1], **Nathan A. Bruender**[2], **Vahe Bandarian**[3], and **R. David Britt**[1]

[1]Department of Chemistry, University of California, Davis, Davis, California 95616, United States

[2]Department of Chemistry and Biochemistry, St. Cloud State University, St. Cloud, Minnesota 56301, United States

[3]Department of Chemistry, University of Utah, Salt Lake City, Utah 84112, United States

Abstract

7-Carboxy-7-deazaguanine (CDG) synthase (QueE), a member of the radical *S*-deoxyadenosyl-L-methionine (SAM) superfamily of enzymes, catalyzes a radical-mediated ring rearrangement required to convert 6-carboxy-5,6,7,8-tetrahydropterin (CPH_4) into CDG, forming the 7-dezapurine precursor to all pyrrolopyrimidine metabolites. Members of the radical SAM superfamily bind SAM to a [4Fe-4S] cluster, leveraging the reductive cleavage of SAM by the cluster to produce a highly reactive 5′-deoxyadenosyl radical which initiates chemistry by H-atom abstraction from the substrate. QueE has recently been shown to use 6-carboxypterin (6-CP) as an alternative substrate, forming 6-deoxyadenosylpterin as the product. This reaction has been proposed to occur by radical addition between 5′-dAdo• and 6-CP, which upon oxidative decarboxylation yields the modified pterin. Here, we present spectroscopic evidence for a kinetically competent 6-CP-dAdo radical. The structure of this intermediate is determined by characterizing its electronic structure by continuous wave and pulse electron paramagnetic resonance spectroscopy.

Graphical Abstract

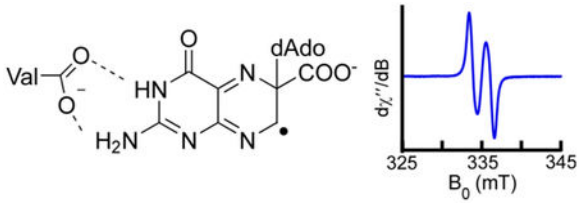

*Corresponding Author: rdbritt@ucdavis.edu, vahe@chem.utah.edu.

Supporting Information: The Supporting Information is available free of charge via the Internet at http://pubs.acs.org. Supplemental information includes the following: LC-MS analysis 6-CP isotopologues, Time dependent formation and decay of 6-CP-Ado•, and additional CW EPR and HYSCORE spectra.

Introduction:

7-Deazapurine containing natural products are found in a variety of biological motifs,[1–2] including the hypermodified tRNA bases queuosine[3] and archaeosine.[4] Queuosine is located in the wobble position of tRNAs bearing His, Tyr, Asp, and Asn with the 5′-GUN-3′ anticodon.[5] The 7-deazapurine moiety that is at the core of all pyrrolopyrimidine nucleosides is derived from GTP in three steps (Scheme 1A).[6–9] The first two are catalyzed by GTP cyclohydrolase I (GCH I) and 6-carboxy-5,6,7,8-tetrahydropterin (CPH_4) synthase (QueD), which convert GTP to CPH_4. In the third step, the radical *S*-deoxyadenosyl-L-methionine (SAM) enzyme 7-carboxy-7-deazaguanine (CDG) synthase (QueE) catalyzes a dramatic and unprecedented heterocyclic rearrangement, converting CPH_4 to CDG.[10] In the reaction, H-atom abstraction at the C-6 position of CPH_4 initiates the reaction where the N on the pyrazine ring is lost as ammonia, forming a pyrrole ring while maintaining the exocyclic carboxyl moiety.[8, 10]

The radical SAM superfamily, of which QueE is a member, was originally identified on the basis of a conserved $CX_3CX\Phi C$ motif, in which Φ is an aromatic residue, and the three cysteine-thiolate side chains each coordinate an iron atom of a site-differentiated [4Fe-4S] cluster.[11] Recent bioinformatics studies have estimated that there are >100,000 members in this radical SAM superfamily.[12] A common theme of enzymes in the superfamily is the reductive cleavage of the [4Fe-4S] cluster-bound SAM to generate a highly reactive oxidant, the 5′-deoxyadenosyl radical (dAdo•) (Scheme 1B), which typically abstracts a H-atom from the specific enzyme's substrate as a central key step in the catalysis.[13]

The X-ray crystal structures of a number of radical SAM enzymes show that they all adopt a structure reminiscent of either a full $(\beta/\alpha)_8$ or partial $(\beta/\alpha)_6$ triose-phosphate isomerase (TIM) barrel fold.[14–32] X-ray structures of QueE from two organisms, *Burkholderia multivorans* and *Bacillus subtilis*, reveal the modes of substrate (CPH_4) and product (CDG) binding (Figure 1A). As in other radical SAM enzymes, the SAM binds through the amino and carboxylate moieties to the unique non-cysteine-ligated iron of the [4Fe-4S] cluster. In the structure of the CPH_4 complex, the C-6 hydrogen, which deuterium labeling studies have shown is abstracted by 5′-dAdo• to initiate catalysis, is within 3.4 Å of the 5′-carbon of SAM.[10, 33]

Recent structural studies with *B. subtilis* homolog and 6-carboxypterin (6-CP; Figure 1C), an CPH_4 analog (Figure 1B) obtained under non-reducing conditions, revealed electron density that was inconsistent with intact SAM and 6-CP.[34] The most reasonable interpretation of the electron density is that the 5′-position of SAM has undergone a nucleophilic addition carboxyl moiety of the 6-CP to displace Met forming 6-carboxypterin-5′-adenosyl ester (6-CP-Ado), Figure 1, D and E. This reaction was also shown to occur *in vitro* using high-resolution mass spectrometry with various isotopically enriched SAM and 6-CP analogs.[34] Interestingly, a different dAdo adduct, 6-deoxyadenosylpterin (6-dAP), is formed *in vitro* under reducing conditions that are required for catalysis. This unusual product, 6-deoxyadenosylpterin (6-dAP), is proposed to form by addition of the 5′-dAdo radical to the 6-position of 6-CP followed by oxidative decarboxylation.[34] Herein we describe the characterization of an intermediate in the reaction

by which QueE produces 6-dAP. The structure of the radical intermediate was determined through continuous wave (CW) and pulse electron paramagnetic resonance spectroscopy measurements. Implications of the intermediate to radical SAM enzymology are discussed.

Methods/Materials:

Chemicals:

6-CP and sodium dithionite were purchased from Sigma-Aldrich. [U-$^{15}N_5$] GTP and [U-^{2}H] GTP were from Cambridge Isotope Labs. PIPES was purchased from Research Products International.

Enzyme Purification:

His_6-tagged QueE from *B. subtilis* used in this investigation was cloned, expressed, and purified as previously described.[34]

Preparation of isotopologues:

SAM was prepared as previously described.[34] [$^{13}C_{10}$] SAM and [U-$^{13}C_7$] 6-carboxypterin were synthesized as previously described.[34] [U-$^{15}N_5$] and [7-^{2}H] 6-carboxypterin were synthesized in the same manner as previously described for [U-$^{13}C_7$] 6-carboxypterin from [U-$^{15}N_5$] GTP and [U-^{2}H] GTP in $^{2}H_2O$ respectively.[34] LC-MS analysis showed that [U-$^{15}N_5$] 6-carboxypterin was 99% pure and 95% enriched with ^{15}N and [7-^{2}H] 6-carboxypterin was 98% pure and 96% enriched with ^{2}H (SI Figure 1).

Electron Paramagnetic Resonance (EPR) Sample Preparation and Spectral Simulations:

All EPR samples were prepared in an anaerobic chamber (Coy Labs, 95% N_2/5% H_2). EPR samples contained 50 mM PIPES•NaOH (pH 7.4), 10 mM DTT, 10 mM sodium dithionite, 2 mM SAM, 2 mM $MgSO_4$, 0.2 mM *B. subtilis* QueE, and 1 mM natural abundance or isotopically enriched 6-CP. For time courses, all components except dithionite and 6-CP were mixed at room temperature (~20 C). Dithionite was then added to this mixture and incubated for 10 min, followed by the initiating the reaction with 6-CP. Reaction mixtures were transferred into 3.8 mm (X-band), 2.0 mm (Q-band) or 1.1 mm (D-band) thin walled quartz EPR sample tubes (Wilmad Glass or Vitrocom) and quenched by freezing in liquid nitrogen after 1, 5, 10, 30, or 60 min incubation. Reactions quenched at 10 min were selected as the standard for samples containing the isotopically enriched 6-CP. In these reactions, the samples were prepared as described above. Samples were stored in liquid nitrogen after freezing. Spectral simulations were performed using the EasySpin 4.0 toolbox in Matlab.[35] In order to ensure the greatest accuracy in our simulations, all data of a specific isotopologue has been simultaneously simulated resulting in simulations for all the experimental data with a single set of parameters. Uncertainty of the hyperfine values were determined by multiple least squares fitting of the data.

X band CW EPR measurements:

Samples for X-band (~9.4 GHz) EPR spectroscopy were measured at the CalEPR center at the University of California, Davis. Continuous wave (CW) spectra were collected using a

Bruker Instruments EleXsys-II E500 CW EPR spectrometer (Bruker Corporation, Billerica, MA) equipped with an Oxford Instruments ESR900 liquid helium cryostat and an Oxford Instruments ITC503 temperature and gas-flow controller. Samples were measured under non-saturating slow-passage conditions using a Super-High Q resonator (ER 4122SHQE). Typical acquisition conditions were: T= 100 K; 9.4 GHz microwave frequency; 3G modulation amplitude; 1 mW microwave power.

Pulse EPR and ENDOR measurements:

All Q-band (34 GHz) pulse EPR studies were carried out at the UC Davis CalEPR center, using a Bruker EleXsys E580 pulse EPR spectrometer equipped with an Oxford-CF935 liquid helium cryostat and an ITC-503 temperature controller. Q-band pulse EPR and Davies Electron Nuclear Double Resonance (ENDOR) spectroscopy were performed using the same E580 EPR spectrometer along with a 1 kW ENI RF amplifier and an R.A. Isaacson-designed cylindrical TE011 resonator[36] adapted for pulse EPR in an Oxford Instruments CF935 cryostat. Davies ENDOR spectra were acquired using the pulse sequence $\pi - t_{RF} - \pi_{RF} - t_{RF} - \pi/2 - \tau - \pi -$echo, where π_{RF} is the optimized RF pulse length and t_{RF} is a fixed delay separating MW and RF pulses.[37] Typical collection conditions were: T=20K, 34.16 GHz microwave frequency, 2.4 mW microwave power, 48 ns inversion (π) pulse, τ =400 ns, RF pulse length: 30 μs (^{13}C), 16 μs (^{1}H), and 60 μs (^{15}N). To avoid saturation of the ENDOR transitions, data were collected using stochastic RF frequency jumping.[38] Hyperfine sublevel-correlation (HYSCORE) spectroscopy was performed using the pulse sequence: $\pi/2$-τ-$\pi/2$-T_1-π-T_2-$\pi/2$-τ-echo.[37] In the HYSCORE experiment, T_1 and T_2 are incremented by 20 ns steps to produce a two dimensional spectrum. D-band (130 GHz) Davies ENDOR spectra were collected on a laboratory-constructed pulse EPR spectrometer[38] using the Davies pulse sequence. Typical collection conditions were: microwave frequency 129.9 GHz, T=30K; 80 ns inversion (π) pulse, 50 μs RF pulse, τ =400 ns. A field sweepable 8-T cryogen-free superconducting magnet (Cryogenic Ltd., London) was used to generate the required magnetic field.

Results:

Observation of a 6-CP based radical intermediate:

EPR studies with QueE have shown that upon reduction with dithionite in the presence of SAM, the [4Fe-4S] cluster presents a rhombic EPR signal and $g_{avg} < 2.0$, as typical for other radical SAM enzymes.[10] By contrast, when QueE is incubated with 6-CP, SAM, and dithionite, an entirely different EPR signal is observed (Figure 2i), which consists of a doublet signal centered at g=2.004 with a ~2 mT peak to peak splitting.[1] The g-value and lack of apparent rhombicity is most consistent with an organic radical, and not a [4Fe-4S] cluster. The formation of the major doublet signal is slow (Figure 2i); it is visible within 1 min after mixing QueE with 6-CP, SAM, and dithionite, and decaying by 120 min (SI Figure 2).[34]

[1]In some samples, we note additional features at 329 mT and 341 mT. However, since these features are not always present and do not change with isotope labeling, we have not investigated these further.

To investigate if the doublet signal corresponds to the elusive 5′-dAdo• radical, samples were prepared with isotopically enriched SAM with the deoxyadenosyl moiety labeled with ^{13}C at all carbon positions ([$^{13}C_{10}$] SAM). As with natural abundance SAM, a doublet signal was also observed with the labeled SAM (Figure 2ii). Since SAM was uniformly labeled with ^{13}C, the absence of substantial changes in the line shape due to hyperfine coupling to a ^{13}C (I=1/2) rules out that the unpaired spin is localized onto the 5′-dAdo scaffold. However, comparison of the spectra obtained with isotopically enriched and natural abundance SAM reveals observable broadening by ~0.3 mT, SI Figure 3, which presumably results from weak coupling of the radical to the deoxyadenosyl moiety.

Pulse electron nuclear double resonance (ENDOR) spectroscopy on the intermediate was carried out to probe for ^{13}C nuclei with couplings too weak to resolve in the CW EPR spectra. The ENDOR experiment uses radio frequency irradiation to modulate the intensity of the observed EPR signal at a stationary magnetic field.[39] The Davies Q-band pulse ENDOR spectrum of the ^{13}C SAM labeled sample, which shows the intensity changes of the EPR signal plotted against the rf excitation frequency (Figure 3A), reveals the presence of a single ^{13}C nucleus coupling associated with the radical intermediate. The spectrum of the doublet is centered at the Larmor frequency for ^{13}C (ν=13.03 MHz at 1217 mT) with a splitting of ~13 MHz. The lower frequency branch of the doublet at 6 MHz is much weaker in intensity than the higher frequency branch due to hyperfine enhancement, an effect which modulates the effective rf field at the spin center leading to different intensities of the ENDOR features.[37] We can simulate the isotopically enriched spectrum in the EasySpin simulation package with a ^{13}C hyperfine tensor of **A** (MHz) = [11.3 11.3 16.0] (Figures 2ii and 3A, red trace). These simulation parameters also reproduce the observed line broadening present in the X-band CW spectrum of the samples with ^{13}C labeled SAM compared to samples with unlabeled SAM, Figure 2ii and SI Figure 3. The overall coupling arises from both isotropic Fermi contact term (A_{iso} = (A_1+A_2+A_3)/3), and anisotropic ($\mathbf{A}_{aniso}$) components that arises from through space coupling ($\mathbf{A}$= A_{iso} +$\mathbf{A}_{aniso}$). Therefore, the strong isotropic component (A_{iso}=12.8 MHz) arises from contact of the ^{13}C nucleus with an orbital containing unpaired spin density. While these data do not unambiguously establish the structure of the radical, they point to the dAdo fragment as being part of the radical species.

To further probe the structure of the radical, continuous wave and pulse EPR experiments were repeated with ^{2}H, ^{15}N, or ^{13}C isotopologues of the 6-CP substrate. When we incubate QueE with unlabeled SAM, [7-^{2}H]-6-CP, and dithionite, the doublet splitting of the radical collapses (Figure 2iii) to a single peak centered at a g = 2.004. While ^{2}H is an I=1 nucleus, the gyromagnetic ratio of deuterium is 6.5-fold smaller than that of protium. Therefore, the loss of the splitting establishes unambiguously that the coupling observed in the spectrum of the unlabeled 6-CP arises from the proton at C-7. With unlabeled 6-CP (Figure 3Bi), ENDOR analysis reveals a broad response from this strongly coupled proton, which is most evident when compared to the parallel ENDOR spectrum from the [7-^{2}H]-6-CP sample (Figure 3Bii) collected under the same conditions. The breadth of the peak from the strongly coupled proton is a result of a high degree of anisotropy in the hyperfine coupling tensor and indeed, the simulation of the CW and ENDOR spectra requires a rhombic hyperfine coupling tensor (in MHz) of **A=** [5 49 80] with a large isotropic coupling constant of A_{iso} =

44.6 MHz, Figure 2i red trace. Additionally, there are a set of peaks centered about the 52 MHz ^{1}H Larmor frequency arising from weakly coupled “matrix” protons that are not affected by the [7-^{2}H]-6-CP labeling. These features can be simulated with three protons (H_a, H_b and H_c) having a hyperfine coupling (in MHz) of $\mathbf{A}(H_a)$ = [5.5 5.5 10], $\mathbf{A}(H_b)$ = [5.5 5.5 2.5], and $\mathbf{A}(H_c)$= [3.3 3.3 0.3].

The radical species derived from [U-$^{15}N_5$]-6-CP isotopologue has no observable changes in the line shape or breadth of the CW spectrum compared to natural abundance 6-CP (Figure 2iv) indicating weak coupling to the nitrogens present in the pterin. To resolve the weak hyperfine couplings to the nitrogens, we used two pulse EPR techniques, ENDOR and HYSCORE, of the I=1/2 ^{15}N nucleus for a more detailed view of this coupling.

Both ^{14}N (I=1) and ^{15}N (I=1/2) nuclei are suitable candidates for ENDOR and HYSCORE spectroscopy having a nuclear spin $I > 0$. However, the nuclear quadrupole of the ^{14}N nucleus can complicate the spectra. Therefore, we obtained Davies ENDOR and HYSCORE spectra of samples prepared with the [U-$^{15}N_5$]-6-CP isotopologue. The Q-band ENDOR spectrum of the [U-$^{15}N_5$]-6-CP isotopologue (Figure 3C) exhibits four partially resolved peaks between 5–10 MHz. The peaks, with a maximal hyperfine coupling of ~10 MHz, are tentatively assigned to the four in-ring nitrogen atoms present in the pterin. Due to the overlap of spectral features we sought to verify the couplings and resolve any anisotropy using HYSCORE. The HYSCORE experiment allows for a two-dimensional analysis of the hyperfine couplings and is helpful for identifying any anisotropy present as well as report the sign of A_{iso} relative to $\mathbf{A}_{aniso}$. The elongated ridge present between 1–10 MHz in the HYSCORE spectrum (SI Figure 4) is due to anisotropy in the coupling originating from the two more strongly coupled nitrogens. We find good agreement in the simulation parameters used in both ENDOR and HYSCORE spectra, reported in Table 1.

We next examined the EPR spectra of QueE incubated with SAM, [U-$^{13}C_7$]-6-CP, and dithionite. The CW spectrum (Figure 2Av) exhibits substantial line broadening and is rich in features as a result of several ^{13}C coupling that cannot be resolved by CW EPR alone. To resolve the hyperfine coupling values for the carbons in the radical, this sample was examined by ENDOR spectroscopy at two frequencies, Q-band (~34 GHz) (Figure 4A) and D-band (~130 GHz) (Figure 4B). This approach allows magnitudes of both strong and moderate couplings to be determined readily when the ENDOR peaks are overlapping, as is the case in the sample with [U-$^{13}C_7$]-6-CP. The advantage of using two frequencies arises from the peak positions in a strong vs weak field limit. In the strong field limit ($\mathbf{A} < 2\nu^{13}$C), the ^{13}C couplings appear as a doublet, centered at the Larmor frequency (ν^{13}C) and split by the magnitude of the hyperfine coupling. In the weak field limit ($\mathbf{A} > 2\nu^{13}$C) the observed peaks are centered at $\mathbf{A}/2$ and split by twice the Larmor frequency. Therefore, at Q-band, where ν^{13}C is ~13 MHz, any couplings larger than ~26 MHz will appear shifted (as is the case with the [U-$^{13}C_7$]-spectrum). In the spectrum at D-band (130 GHz microwave, ~4.6T magnetic field), all ^{13}C couplings are expected to follow the strong field limit where all doublets are centered at the Larmor frequency and peaks split by the magnitude of the hyperfine coupling. Using the two frequencies, we are able to determine if what appears as a shoulder in one spectrum is due to anisotropy in the hyperfine tensor, or a partially overlapping peak. We observe five unique carbon couplings by ENDOR and can simulate

the spectra taken at Q- and D- band with the values reported in Table 1. We note that there is no observable *g*-anisotropy at X-, Q-, and D-band. Lack of observable *g*-anisotropy at the frequencies examined is not unexpected, and indicates a radical with little spin density delocalized on atoms other than carbon. Another example of a type of biological radical with little *g*-anisotropy is the tryptophan radical, in the Trp radical the small *g*-anisotropy is only detected at very high frequency (>285 GHz) and field (>10.2 T).[40]

While spectral simulations can be made of the observed ENDOR peaks, the CW spectrum is poorly simulated, SI Figure 5. To simulate the CW, one additional strongly coupled, very anisotropic, carbon is required having a hyperfine coupling tensor of **A** (MHz) = [29 92.3 160]. Due to the anisotropy of this tensor, one would expect the resulting ENDOR intensity to be spread out and difficult to detect, and indeed the resulting ENDOR simulations, Figure 4A and B, show a broad peak near the baseline.

QueE has been shown to turnover with 6-CP under reducing conditions to form 6-deoxyadenosylpterin (6-dAP).[34] The doublet in the spectrum arising from the hyperfine coupling to the proton at C-7 of 6-CP is significant as addition of the 5′-dAdo• to the C-6 position of 6-CP would lead to an adduct with unpaired spin density at C-7. The 6-CP adduct, however, can exist in large number of tautomeric states, which would differentially impact the allowed resonance structures and the corresponding spin density distributions. Nevertheless, one would predict that the large magnitude of the coupling to the C-7 proton suggests significant spin density (53–80%) resides at the C-7 carbon based on the McConnell relationship, which relates the isotropic hyperfine coupling of a proton to the spin density at the carbon to which it is attached.[41] In the prototypical methyl radical[42], the unpaired spin is localized entirely to a p_z orbital of carbon. This localized spin results in proton hyperfine coupling values (A_{iso}) of ~70 MHz and a ^{13}C hyperfine coupling value (A_{iso}) of ~100 MHz. Using these values, and our experimentally derived C-7 proton hyperfine coupling values (A_{iso}=44.6 MHz, calculated from the tensor [5 49 80]), one would predict ~63% spin density (A_{iso} ~ 63 MHz) in the C-7 p_z orbital. The measured ^{13}C hyperfine coupling with a tensor of [44.5 54 57] (A_{iso} = 51.8 MHz) agrees well with this estimate provided by both the calculated values using the McConnell equation and comparison of the methyl radical. The weaker but measurable coupling to the 5′-Ado clearly shows that the radical intermediate is covalently attached to the cofactor. Finally, the substantial couplings to ^{13}C nuclei within the 6-CP ring system are consistent with coupling to C-6, and potentially other carbon centers where there is significant spin density. A quantitative description of the structure is difficult because of the large number of tautomeric states of the radical intermediate, which would have distinct delocalization properties. Nevertheless, the data permit one to propose that the intermediate being observed forms by dAdo• addition at C-6, generating a species with substantial spin density at C-7. The mechanism by which the radical undergoes decarboxylation remains to be determined.

Discussion:

Here we present evidence for a radical intermediate following 5′-dAdo• addition at C-6 of 6-CP. Using isotopologues of 6-CP and the deoxyadenosyl moiety of SAM we have measured the hyperfine couplings, which report on the localization of the unpaired spin

density in the intermediate. Of note is the large hyperfine coupling from the C-7 proton, small hyperfine couplings to the nitrogens, and the presence of modest hyperfine coupling to a carbon of the dAdo adduct. In contrast to the 6-CP adduct observed here, the pterin radical observed in the reaction of (6*R*)-5,6,7,8-tetrahydropterin (H_4B) in nitric oxide synthase (NOS) carries delocalized unpaired spin density on the pterin rings resulting in additional spin density on the in-ring nitrogens.[43] Interestingly, there is some similarity in the radical intermediate in the radical SAM enzymes Cfr and RlmN.[44] This intermediate is formed by addition of a thio-methyl radical to an sp^2 carbon center. Like the 6-CP-dAdo radical, the radical intermediate has a majority of the unpaired spin is localized to atom adjacent to the site of addition.[44]

The X-ray crystal structures of QueE highlight that the substrate is bound in the active site such that it places the C-6 hydrogen of CPH_4 within easy reach of the dAdo formed by reductive cleavage of SAM.[33–34] The resulting radical intermediate is thought to undergo a radical-mediated ring contraction, resulting in a *gem*-aminocarboxylate intermediate, Scheme 2. The mechanism by which this putative intermediate is converted to the CDG product is not known; however, studies with CPH_4 isotopologs carrying deuterium at C7 in either the *proS* or *proR* positions have shown that the proton abstraction is stereoselective.[10] Interestingly, the pyrimidine ring of the ligands interact through the exocyclic amino and endocyclic nitrogen with the C-terminal carboxylate of the protein. In the context of the studies in this paper where the data show that 6-CP radical adduct appears to maximize spin density at C-7, the interaction could differentially stabilize tautomeric states of 6-CP that minimize delocalization (see Scheme 2**: 6-CP-Ado**). Moreover, this interaction may also play a role in the second half of the catalytic cycle, which has been proposed to be elimination of the amino group and deprotonation of an intermediate *gem*-aminocarboxylate intermediate to form CDG. Studies that probe the role of this and other residues that are in the vicinity of the putative *gem*-aminocarboxylate intermediate are currently in progress.

In the absence of a suitable hydrogen atom to abstract, we observe that radical SAM chemistry in QueE follows a different path. The close proximity of the dAdo• and the 6-CP would permit radical addition, leading to formation of the observed intermediate. The mechanism by which the intermediate undergoes decarboxylation to form 6-dAP remains to be determined.

It is now established that the dAdo radical moiety itself can add to sp^2 hybridized carbon centers, such as the reaction catalyzed by MqnE which catalyzes the formation of aminofutalosine.[45–46] The observation of differential reactivity of QueE with 6-CP in the presence and absence of reductant underscores the plasticity that must be inherent to radical SAM enzymes. The X-ray crystal structures of QueE highlight how its active site is finely-tuned to promote abstraction of the H-atom at C-6 of the substrate. However, in the absence of a hydrogen atom within van der Waals distance of the 5′-dAdo•, it undergoes radical addition. This suggests that the catalytic trajectory followed by QueE and other radical SAM enzymes could include very diverse reactions, whereby proximity dictates the catalytic course. In QueE, when 6-CP is used under non-reducing conditions, the carboxylate of the analog is within range of SAM to form an ester adduct – a reaction that has yet to be documented with the natural substrate. It remains to be seen if all members of the radical

SAM superfamily catalyze entirely radical-mediated transformations, or perhaps if some have evolved to take advantage of an activated SAM that can react by polar or radical means. The recent studies with RlmN and Cfr highlight just such a case in a naturally occurring enzyme and we posit that as additional members of the superfamily are characterized, that the reaction scope of this superfamily will expand.[28, 47] What is becoming clear from studies of both natural radical SAM reactivity and the promiscuous activities of these proteins is that the breadth of chemistry is like to be much broader in this large and growing superfamily.

Supplementary Material

Refer to Web version on PubMed Central for supplementary material.

Funding/Acknowledgements:

The work reported in this publication was supported by National Institutes of General Medical Sciences of the National Institutes of Health grant GM-104543 (R.D.B.) and GM-72623 (V.B.). The content is solely the responsibility of the authors and does not necessarily represent the official views of the National Institutes of Health.

References:

1. Suhadoln Rj; Uematsu T, J. Biol. Chem 1970, 245, 4365–&. [PubMed: 5498424]
2. McCarty RM; Bandarian V, Bioorg. Chem 2012, 43, 15–25. [PubMed: 22382038]
3. Kasai H; Oashi Z; Harada F; Nishimura S; Oppenheimer NJ; Crain PF; Liehr JG; von Minden DL; McCloskey JA, Biochemistry 1975, 14, 4198–208. [PubMed: 1101947]
4. Gregson JM; Crain PF; Edmonds CG; Gupta R; Hashizume T; Phillipson DW; McCloskey JA, J. Biol. Chem 1993, 268, 10076–10086. [PubMed: 7683667]
5. Harada F; Nishimura S, Biochemistry 1972, 11, 301–+. [PubMed: 4550561]
6. McCarty RM; Bandarian V, Chem. Biol 2008, 15, 790–8. [PubMed: 18721750]
7. Phillips G; El Yacoubi B; Lyons B; Alvarez S; Iwata-Reuyl D; de Crecy-Lagard V, J. Bacteriol. 2008, 190, 7876–84. [PubMed: 18931107]
8. McCarty RM; Somogyi A; Lin G; Jacobsen NE; Bandarian V, Biochemistry 2009, 48, 3847–52. [PubMed: 19354300]
9. McCarty RM; Somogyi A; Bandarian V, Biochemistry 2009, 48, 2301–3. [PubMed: 19231875]
10. McCarty RM; Krebs C; Bandarian V, Biochemistry 2013, 52, 188–98. [PubMed: 23194065]
11. Sofia HJ; Chen G; Hetzler BG; Reyes-Spindola JF; Miller NE, Nucleic Acids Res. 2001, 29, 1097–1106. [PubMed: 11222759]
12. Akiva E; Brown S; Almonacid DE; Barber AE, 2nd; Custer AF; Hicks MA; Huang CC; Lauck F; Mashiyama ST; Meng EC; Mischel D; Morris JH; Ojha S; Schnoes AM; Stryke D; Yunes JM; Ferrin TE; Holliday GL; Babbitt PC, Nucleic Acids Res. 2014, 42, D521–30. [PubMed: 24271399]
13. Shisler KA; Broderick JB, Curr. Opin. Struct. Biol 2012, 22, 701–10. [PubMed: 23141873]
14. Layer G; Moser J; Heinz DW; Jahn D; Schubert WD, EMBO J 2003, 22, 6214–24. [PubMed: 14633981]
15. Berkovitch F; Nicolet Y; Wan JT; Jarrett JT; Drennan CL, Science 2004, 303, 76–9. [PubMed: 14704425]
16. Forouhar F; Arragain S; Atta M; Gambarelli S; Mouesca JM; Hussain M; Xiao R; Kieffer-Jaquinod S; Seetharaman J; Acton TB; Montelione GT; Mulliez E; Hunt JF; Fontecave M, Nat. Chem. Biol 2013, 9, 333–8. [PubMed: 23542644]
17. Benjdia A; Heil K; Barends TR; Carell T; Schlichting I, Nucleic Acids Res. 2012, 40, 9308–18. [PubMed: 22761404]

18. Zhang Y; Zhu X; Torelli AT; Lee M; Dzikovski B; Koralewski RM; Wang E; Freed J; Krebs C; Ealick SE; Lin H, Nature 2010, 465, 891–6. [PubMed: 20559380]
19. Suzuki Y; Noma A; Suzuki T; Senda M; Senda T; Ishitani R; Nureki O, J. Mol. Biol 2007, 372, 1204–14. [PubMed: 17727881]
20. Hanzelmann P; Schindelin H, Proc. Natl. Acad. Sci. U.S.A 2006, 103, 6829–34. [PubMed: 16632608]
21. Goldman PJ; Grove TL; Sites LA; McLaughlin MI; Booker SJ; Drennan CL, Proc. Natl. Acad. Sci. U.S.A 2013, 110, 8519–24. [PubMed: 23650368]
22. Goldman PJ; Grove TL; Booker SJ; Drennan CL, Proc. Natl. Acad. Sci. U.S.A 2013, 110, 15949–54. [PubMed: 24048029]
23. Coquille S; Roux C; Mehta A; Begley TP; Fitzpatrick TB; Thore S, J. Struct. Biol 2013, 184, 438–44. [PubMed: 24161603]
24. Harmer JE; Hiscox MJ; Dinis PC; Fox SJ; Iliopoulos A; Hussey JE; Sandy J; Van Beek FT; Essex JW; Roach PL, Biochem. J 2014, 464, 123–33. [PubMed: 25100160]
25. Nicolet Y; Zeppieri L; Amara P; Fontecilla-Camps JC, Angew. Chem., Int. Ed 2014, 53, 11840–4.
26. Nicolet Y; Pagnier A; Zeppieri L; Martin L; Amara P; Fontecilla-Camps JC, ChemBioChem 2015, 16, 397–402. [PubMed: 25504963]
27. Rohac R; Amara P; Benjdia A; Martin L; Ruffie P; Favier A; Berteau O; Mouesca JM; Fontecilla-Camps JC; Nicolet Y, Nat. Chem 2016, 8, 491–500. [PubMed: 27102684]
28. Schwalm EL; Grove TL; Booker SJ; Boal AK, Science 2016, 352, 309–12. [PubMed: 27081063]
29. Bridwell-Rabb J; Zhong A; Sun HG; Drennan CL; Liu HW, Nature 2017, 544, 322–326. [PubMed: 28346939]
30. Dinis P; Suess DL; Fox SJ; Harmer JE; Driesener RC; De La Paz L; Swartz JR; Essex JW; Britt RD; Roach PL, Proc. Natl. Acad. Sci. U.S.A 2015, 112, 1362–7. [PubMed: 25605932]
31. Vey JL; Drennan CL, Chem. Rev 2011, 111, 2487–506. [PubMed: 21370834]
32. Dowling DP; Vey JL; Croft AK; Drennan CL, Biochim. Biophys. Acta 2012, 1824, 1178–95. [PubMed: 22579873]
33. Dowling DP; Bruender NA; Young AP; McCarty RM; Bandarian V; Drennan CL, Nat. Chem. Biol 2014, 10, 106–12. [PubMed: 24362703]
34. Bruender NA; Grell TA; Dowling DP; McCarty RM; Drennan CL; Bandarian V, J. Am. Chem. Soc 2017, 139, 1912–1920. [PubMed: 28045519]
35. Stoll S; Schweiger A, J. Magn. Reson 2006, 178, 42–55. [PubMed: 16188474]
36. Flores M; Isaacson RA; Calvo R; Feher G; Lubitz W, Chem. Phys 2003, 294, 401–413.
37. Schweiger A; Jeschke G, Principles of Pulse Electron Paramagnetic Resonance. Oxford University Press: UK, 2001.
38. Bruggemann W; Niklas JR, J. Magn. Reson. A 1994, 108, 25–29.
39. Kulik L; Lubitz W, Photosynth. Res 2009, 102, 391–401. [PubMed: 19184518]
40. Stoll S; Shafaat HS; Krzystek J; Ozarowski A; Tauber MJ; Kim JE; Britt RD, J. Am. Chem. Soc 2011, 133, 18098–101. [PubMed: 22007694]
41. Mcconnell HM, J. Chem. Phys 1956, 24, 764–766.
42. Cole T; Pritchard HO; Davidson NR; McConnell HM, Mol. Phys 1958, 1, 406–409.
43. Stoll S; NejatyJahromy Y; Woodward JJ; Ozarowski A; Marletta MA; Britt RD, J. Am. Chem. Soc 2010, 132, 11812–23. [PubMed: 20669954]
44. Grove TL; Livada J; Schwalm EL; Green MT; Booker SJ; Silakov A, Nat. Chem. Biol 2013, 9, 422–7. [PubMed: 23644479]
45. Mahanta N; Fedoseyenko D; Dairi T; Begley TP, J. Am. Chem. Soc 2013, 135, 15318–21. [PubMed: 24083939]
46. Joshi S; Mahanta N; Fedoseyenko D; Williams H; Begley TP, J. Am. Chem. Soc 2017, 139, 10952–10955. [PubMed: 28701039]
47. Boal AK; Grove TL; McLaughlin MI; Yennawar NH; Booker SJ; Rosenzweig AC, Science 2011, 332, 1089–1092. [PubMed: 21527678]

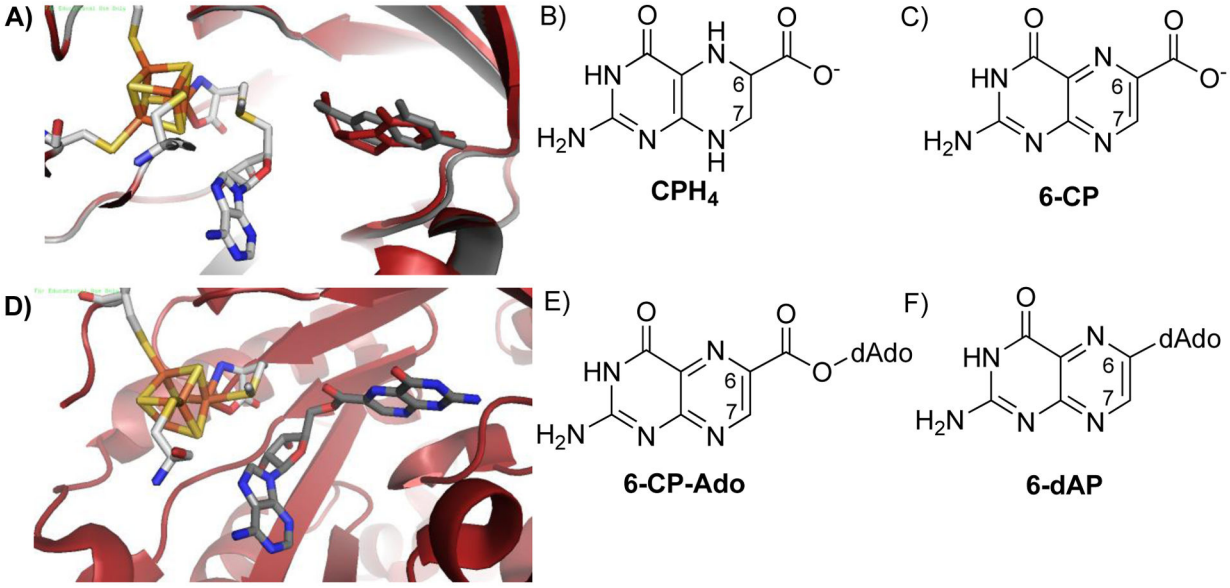

Figure 1:

A): Superimposed crystal structure models of QueE (PDB: 4NJG, 4NJI) with either 6-carboxy-5,6,7,8-tetrahydropterin (CPH_4; Red) or 6-carboxypterin (6-CP; Grey). Lewis structure of the native substrate CPH_4 (**B**) and the substrate analog 6-CP (**C**). **D**) Crystal structure model of QueE (PDB:5TH5) with the 6-carboxypterin-5′-deoxyadenosyl ester (6-CP-Ado). **E**) Lewis structure of the product 6-CP-Ado **F**) Proposed structure of the 6-deoxyadenosyl pterin (6-dAP) product following dAdo addition and oxidative decarboxylation

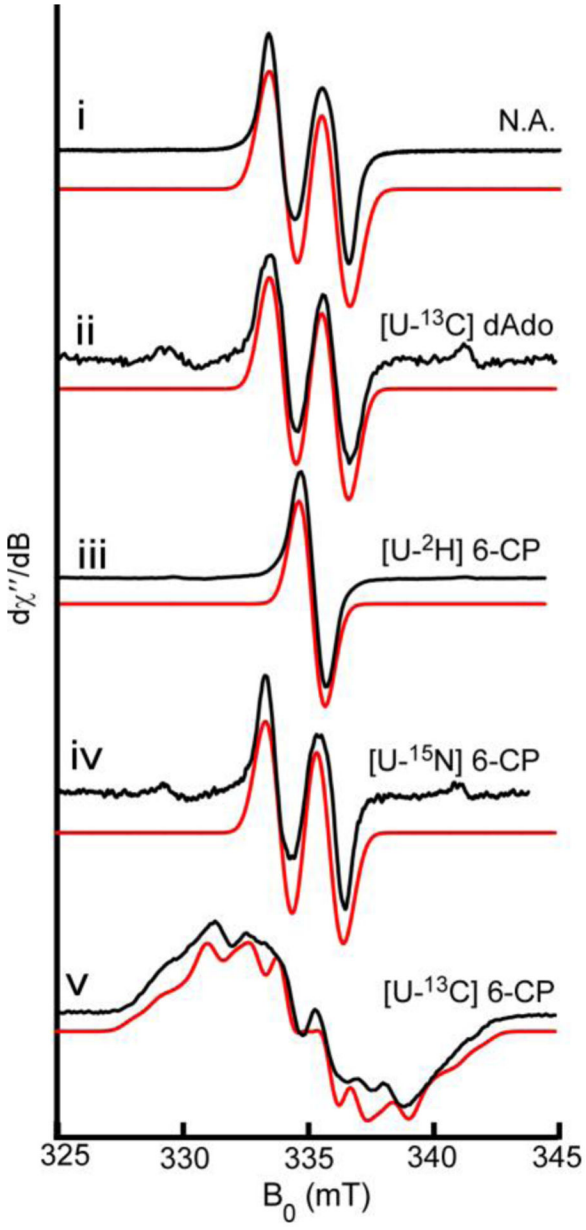

Figure 2:

i) Continuous-wave (CW) X-band (9.4 GHz) EPR spectra of the 6-CP radical intermediate (6-CP-dAdo•) formed when QueE is incubated with dithionite,6-CP, and SAM (Black) along with simulations of the spectra (red). Simulation parameters are reported in Table 1. The remaining spectra are the same reaction conditions as *i*, but using various isotopologues of either SAM or 6-CP presented as follows: *ii*) Natural abundance ([NA])6-CP, [U-$^{13}C_{10}$] dAdo of SAM. *iii*) [U-^{2}H] 6-CP, [NA] SAM, *iv*) [U-$^{15}N_5$] 6-CP, [NA]-SAM, *v*) [U-$^{13}C_7$] 6-CP, [NA]-SAM. Simulated hyperfine couplings are reported in Table 1.

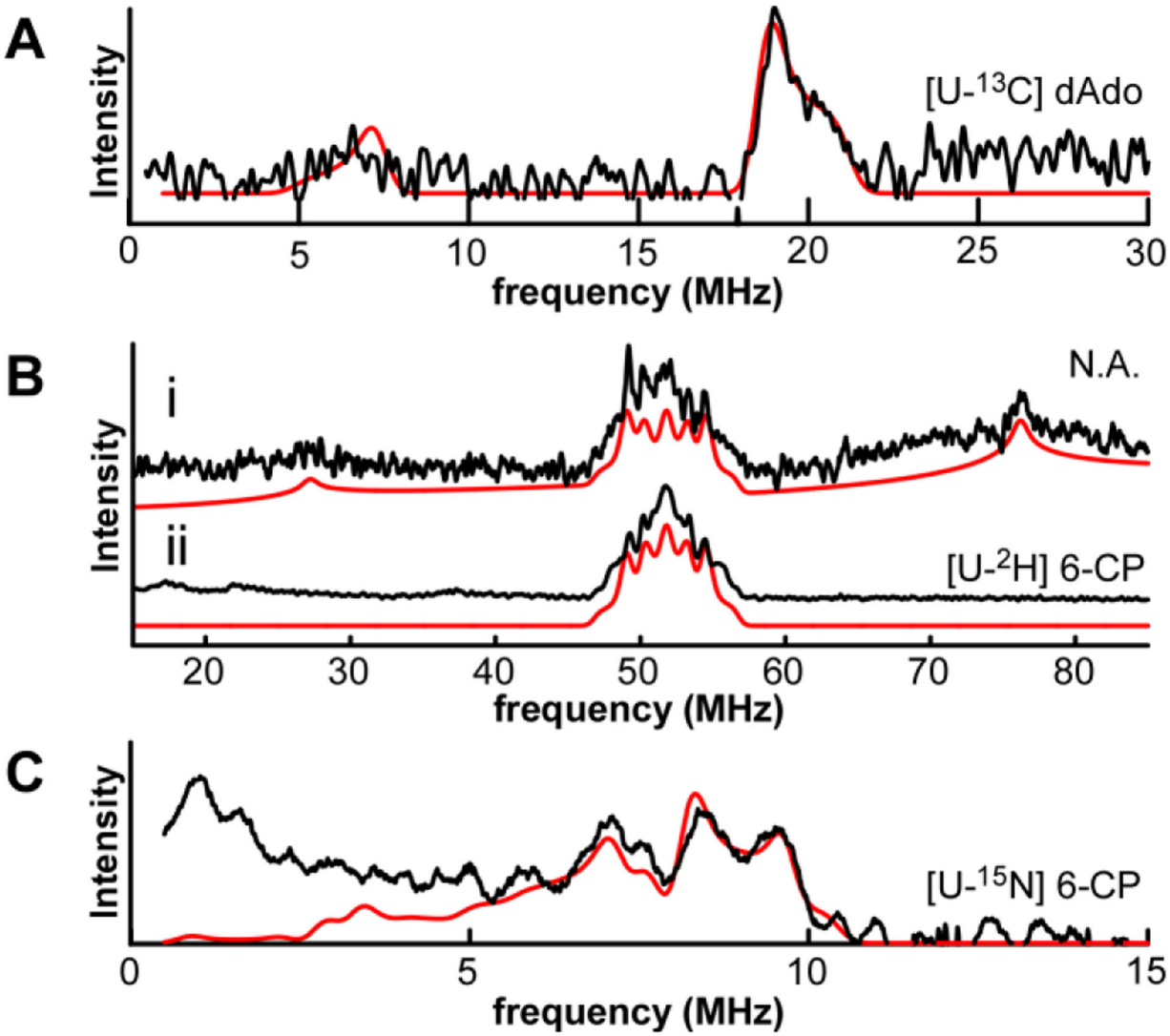

Figure 3:

Davies ENDOR of the 6-CP radical intermediate (6-CP-dAdo) formed when QueE is incubated with dithionite, 6-CP, and [U-$^{13}C_{10}$] dAdo SAM, **A**, (Black) with simulations of the spectrum (Red). The peaks arising from the [U-$^{13}C_{10}$] dAdo fragment are centered at the Larmor frequency for ^{13}C (13 MHz) and split by ~13 MHz. **B**) Davies ENDOR spectra of the 6-CP-dAdo radical when QueE is incubated with dithionite, [NA] SAM and either [7-^{1}H]-6-CP (*i*, Black) or [7-^{2}H]-6-CP (*ii*, Black) along with simulations of the protons in Red. The observed proton couplings are centered at the Larmor frequency for the proton, ~52 MHz and split by the strength of the hyperfine coupling. **C**) Davies ENDOR spectra of the 6-CP-Ado radical when QueE is incubated with dithionite, [NA] SAM, and [U-$^{15}N_5$]-6-CP (Black) along with simulations of the spectrum in Red. The observed nitrogen couplings are centered at the Larmor frequency for ^{15}N (~5 MHz) and split by the strength of the hyperfine coupling, with a maximal splitting of ~10 MHz. Simulation parameters are reported in Table 1.

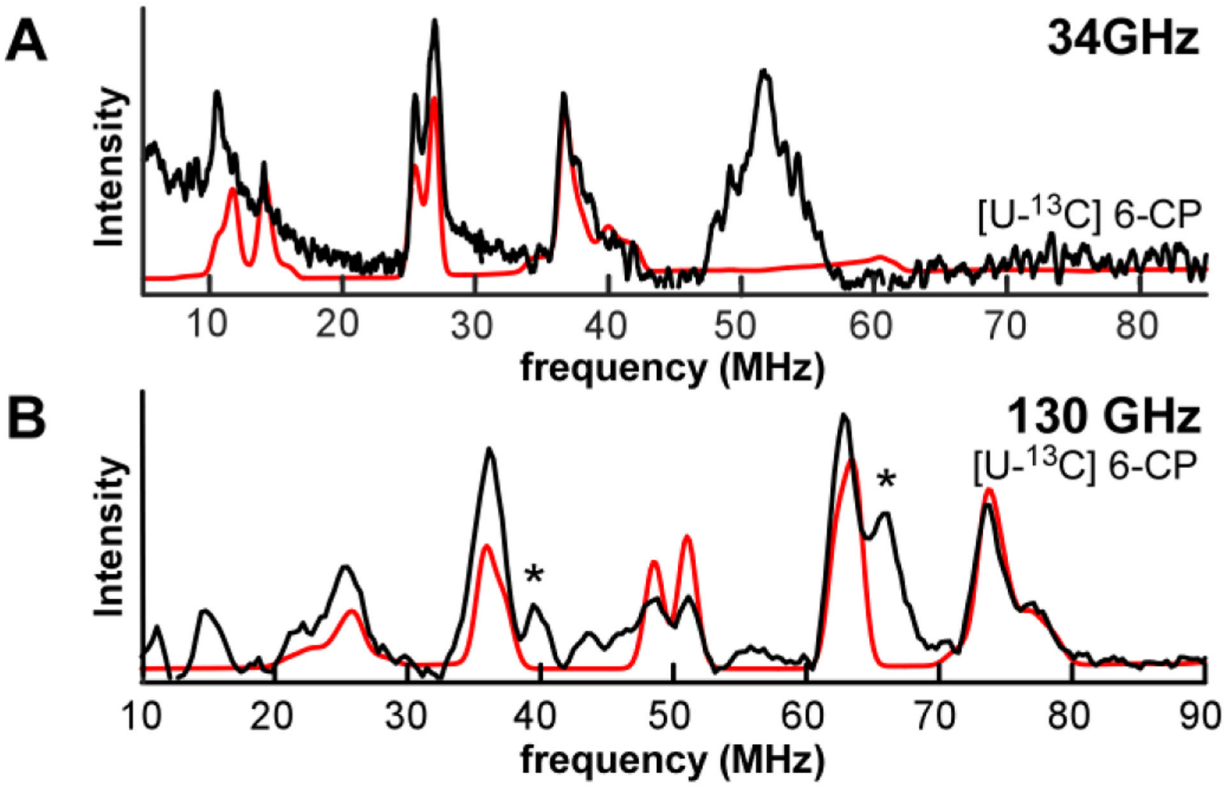

Figure 4:

Davies ENDOR of the radical intermediate formed when QueE is incubated with dithionite, [NA] SAM, and [U-$^{13}C_7$] 6-CP (Black) with simulation of the spectra (red) collected at Q-band (**A**, 34 GHz) and D-band (**B**; 130 GHz). The Larmor frequency for ^{13}C is ~13 MHz and ~50 MHz at Q and D band respectively. The peak at ~52 MHz at Q-band is due to weakly coupled matrix protons, the 3rd and 5th harmonic of the matrix proton peak is visible at D-band (*).

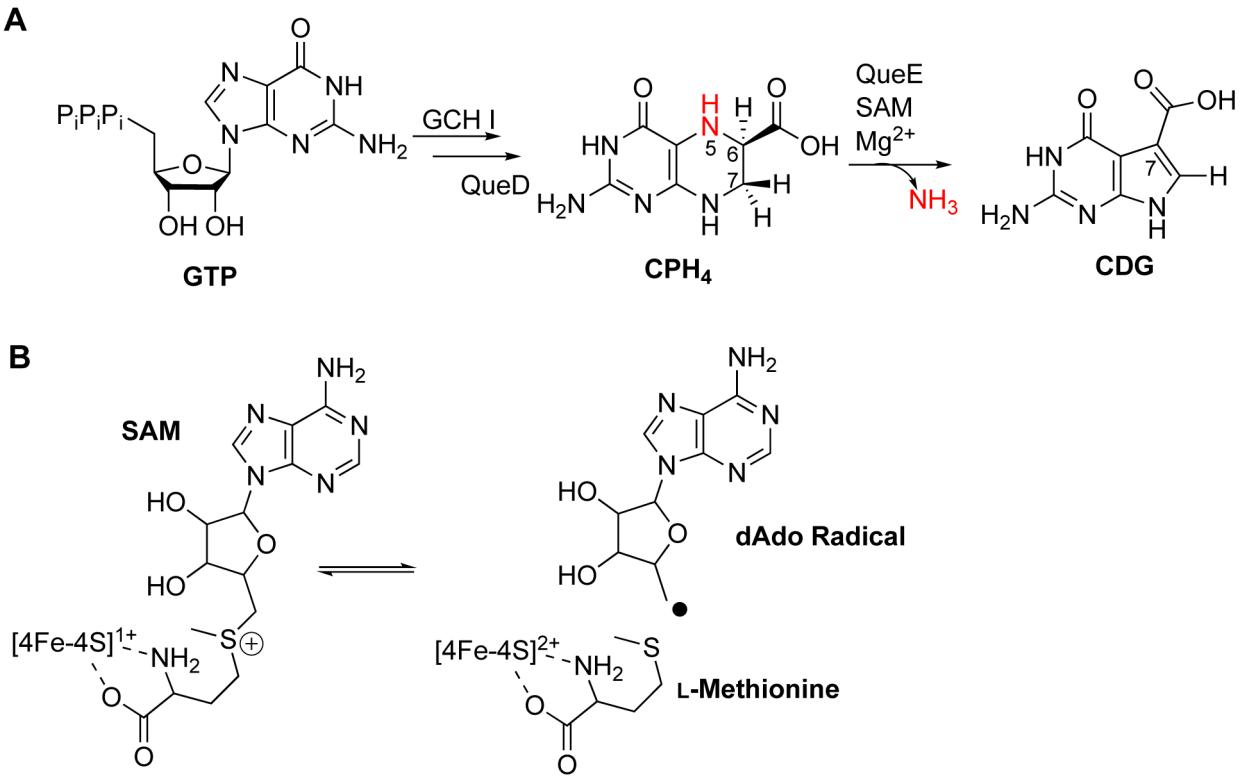

Scheme 1:

A) The 7-deazapurine CDG is formed in 3 steps from GTP. The third step, a ring condensation reaction, is catalyzed by the radical SAM enzyme QueE. **B)** Typical dAdo• formation in radical SAM family enzymes where the 5' C of the deoxyadenosine fragment is homolytically cleaved from the methionine fragment.

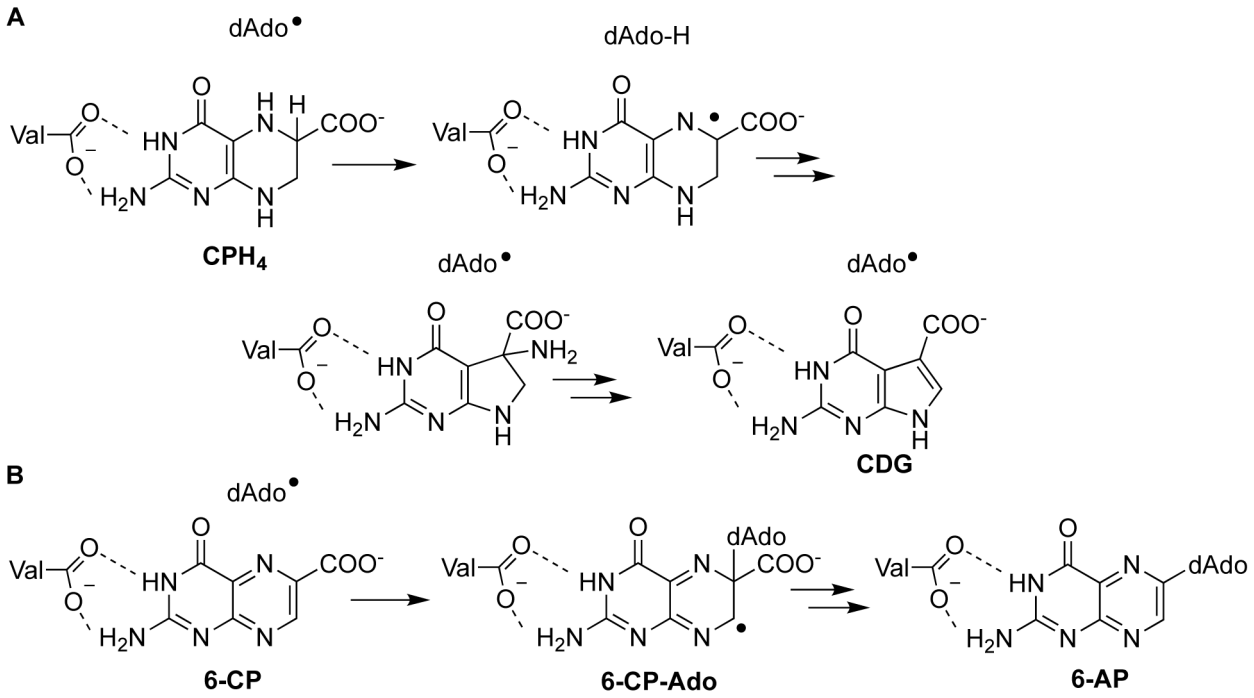

Scheme 2:

A) In the mechanism of CDG formation by QueE, CPH_4 is thought to undergo a radical-mediated ring contraction, resulting in a *gem*-aminocarboxylate intermediate. **B)** The proposed mechanism and intermediate for dAdo• addition to C-6 of 6-carboxypterin. The product of the reaction (6-deoxyadenosyl pterin) has been identified previously by mass spectrometry.[34]

Table 1:

Hyperfine values* (in MHz) from Experimental simulations

	A_1	A_2	A_3
C7-H	5.0 +/− 3.0	49 +/− 1.0	80 +/− 5.0
H_a	5.5	5.5	10
H_b	2.5	5.5	5.5
H_c	0.3	3.3	3.3
5′C-dAdo	11.3	11.3	16.0
C	29.0 +/− 1.2	92.3 +/− 2.6	160 +/− 9.8
C	44.5 +/− 1.5	54.0 +/− 1.0	57.0 +/− 1.0
C	47.0	47.0	50.5
C	24.7	24.7	26.7
C5	28.0	28.0	28.0
C6	1.4	3.5	3.5
N1	−1.5	−1.5	3.0
N2	2.7	2.7	−5.2
N3	1.5	1.5	−3.0
N4	−2.5	−2.5	5.0

* Unless indicated, all uncertainties of the simulated hyperfine values are < +/− 0.5 MHz